Chapter 3

Simulator model derivation

3.1 Introduction

This section deals with the identification of models that are deemed necessary to adequately simulate the thickness profile behaviour of the strip as well as the tension in the sheet whilst rolling. Nonlinear and linear model derivations are shown and some modelling choices are motivated for these models. In this chapter use will be made of general rolling terms. Some of these terms are defined in Appendix A.

3.2 Nonlinear models

The hot rolling mill process is a very complex process to model. The complexity is dependent on the desired capability and accuracy of the mill simulator. Most of the process variables are implicit functions of other process variables, requiring iterative numerical solution methods. The main protagonist of the rolling process is temperature [31], and temperatures of the strip and the rollers influence rolling variables such as the rolling force, rolling torque, crown, and mechanical properties of the product to name a few. The heat transfer problem associated with the Steckel hot rolling mill is very complex [32, 33], and some aspects of this problem will be discussed later in this chapter.

The models identified in this dissertation and their relative dependencies are shown in figure 3.1. The models and their function as part of the simulator can be described as:

1. **Roll gap model:** The roll gap model predicts the specific rolling load across the width of the strip. This model forms the connecting block between all the possible models of the simulator.

2. **Stand model:** This model describes the elastic stretch of the mill stand due to the rolling of the strip as well as the work roll and back-up roll interface flattening. The result is a deviation

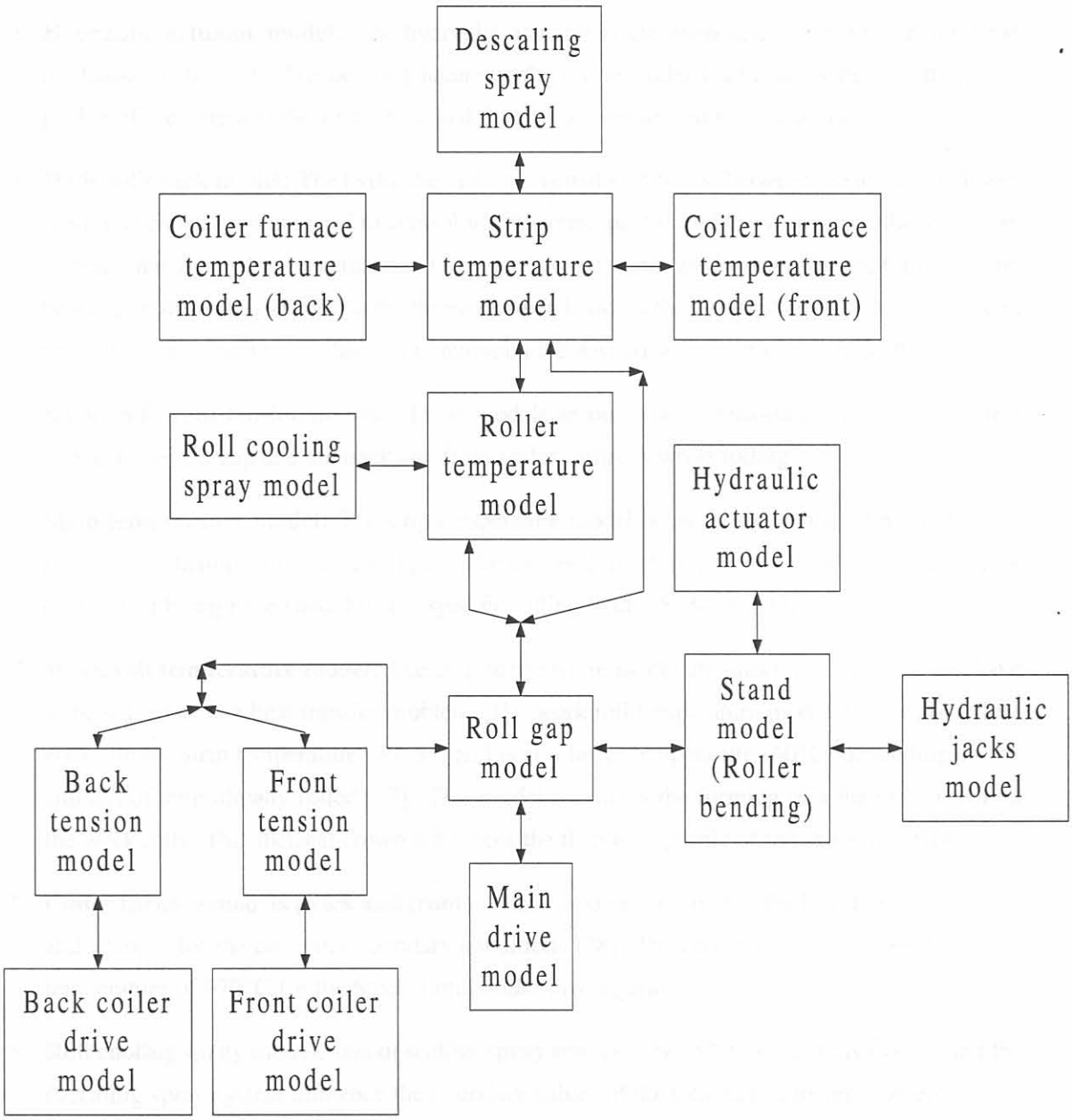

Figure 3.1: Models identified in order to constitute a comprehensive nonlinear mill simulator.

in the draft from the setup reduction draft. The roll bending phenomena of the rollers are incorporated in the stand model. The modelling of the bending phenomena adds the capability of strip thickness profile simulation to the mill simulator. This model can be 3-dimensional or 2-dimensional as shown in [10]. The 2-dimensional model's coordinates are perpendicular and form a yz plane to the rolling direction (x) with the origin chosen at the center of the roll gap.

3. **Hydraulic actuator model:** The hydraulic actuator is the main actuator used to control the thickness of the strip. The bending nature of the rollers under load assures that the thickness profile of the strip and the strip shape and flatness are influenced by this actuator.

4. **Hydraulic jack model:** The hydraulic jacks are actuators situated between the upper and lower work roll chocks and are used to control the thickness profile and the strip shape/flatness more directly than the hydraulic actuators. These jack actuators are used to compensate for the elastic bending of the rollers as well as the thermal crown build on the work rollers, by striving to bend the rollers in a counterwise fashion to maintain the desired strip profile and shape/flatness.

5. **Back and Front tension models:** These models account for the tension behaviour in the strip between the roll gap and the back and front coiler furnaces while rolling.

6. **Strip temperature model:** The strip temperature model is necessary to find an accurate temperature prediction value in the roll gap. The temperature of the sheet influences the yield stress of the steel being rolled and thus the specific rolling load [28, 34, 35, 36, 11].

7. **Work roll temperature model:** The strip temperature model and this model interact and have to be solved as one heat transfer problem. The work roll temperature model has a roll chilling effect on the strip temperature [30, 32] and is at a lower temperature (60°C) depending on the amount of strip already rolled [37]. This model simulates the forming of a thermal crown on the work rolls. This thermal crown influences the thickness profile of the sheet adversely.

8. **Coiler furnace models (back and front):** These models form part of the heat transfer problem and account for the changing boundary conditions [38]. The coiler furnaces are regulated at a temperature of 970°C for the Steckel mill under investigation.

9. **Roll cooling spray model, and descaling spray model:** The roll cooling spray system and the descaling spray system influence the boundary values of the total heat transfer problem.

10. **Mill drive and motor model:** The main drive model incorporates the motor dynamics into the problem. With this model a controller can be designed using the current of the motor in order to control the roll speed and the rolling torque. This model can also be used to investigate the rotational vibration of the connecting spindles on the plastic deformation process in the roll gap [39]. In [40], this mill chattering effect is noted as one of the causes of the asymmetrical vertical displacement for a 2-dimensional stand model.

11. **Back coiler and front coiler drive and motor models:** Two similar motors are used for each coiler and these models will be essentially the same. These two models will also be similar to the main mill drive motor model. These models also relate the speed of the coilers to the motor dynamics and drive dynamics. The limitation of the drive motor can place a limit on the amount of tension control that can be applied.

Not all of these identified models will be modelled in this dissertation. The following models will not be modelled, and the influence on the simulator this lack of modelling will have as well as possible means for compensating for these deficiencies are as follows:

- **Temperature models:** Although temperature was identified as an important parameter, the modelling of the heat transfer problem is too complex for the proposed investigation. The necessary temperature inputs for the simulator are obtained by conditioning practical plant data of the Steckel hot rolling mill under investigation.
- **Main Mill Drive:** The main mill drive speed is not considered as a manipulated variable in this dissertation. Little insight other than the effect of torsional vibrations of the spindles on the roll gap deformation process could be gained by modelling the main mill drive and its connecting work roll shafts in detail.
- **Coiler Motor Drives:** The dynamics of the coiler motors and their loads, which they drive have large inertias that limit the severity of the control action that can be taken for tension control, e.g. speed up/down of the coiler drums. The modelling might be deemed necessary in order to identify possible velocity actuator limits.
- **Hydraulic Jack models:** The simulator developed in this dissertation is not aimed at investigating profile and shape control methods, although some fundamental theory is addressed and some initial modelling is done concerning strip profile and shape issues. In this dissertation these actuators are modelled as discrete spring elements forming part of the stand model.

In the rest of this chapter, nonlinear and linear models for the roll gap, rolling mill stand and strip tension will be derived and an introduction to the heat transfer problem will be discussed.

3.3 Roll gap model

3.3.1 Introduction

Roll gap models can be divided into two groups, namely analytical rolling theory models and numerical Finite Element models. Usually the analytical models is static used for predicting the rolling force

and torque. The Finite Element models either predicts the rolling force and torque or the material behaviour.

Many roll gap models of varying degree of complexity exist in the literature, and the roll gap model is constantly refined and the current trend is to use Finite Element Methods (FEM) to solve the stress-strain partial differential equation model of the roll gap in order to model the plastic metal flow through the roll gap and the microstructure evaluation of the material [36, 41, 42, 43].

The pioneering work on analytical rolling theory models was done by Siebel and Kármán in 1924 and 1925 [28, 44]. Orowan (1943) extended this work and based his analysis on a simplifying assumption that the deformation in the roll gap resembles the compression between rough inclined plates [44]. A similar problem was solved partially by Nadai in 1931. Sims (1954) simplified Orowan's differential equation model by solving the differential equation for certain rolling conditions, for example rolling where sticking friction is assumed [44]. Current research on analytical rolling theory models focuses on special investigations on the roll gap geometry and the angle at which the strip enters the roll gap. One such example of roll gap geometry investigation is discussed in the article by Fleck et al. [45] dealing with cold rolling modelling.

It must be stressed that the Orowan roll gap model is used as a benchmark to validate the performance of other analytical models, such as Sims's model [44] and the Ford and Alexander model [46], as well as FEM models [36]. The theory of plasticity [47] can be used to model the plastic flow through the roll gap and these models are then solved using FEM [41, 42, 43]. These static models accurately describe the stress, the strain and the strain rate which the metal is subjected to by solving the partial differential equations such as the strain rate tensor. For the mechanics of engineering metals (yield criteria, structural analysis, plasticity) the interested reader is referred to [47, 48].

The thermal analysis combined with the roll gap analysis was done by Samarasekera et al. [33] using a FEM model. This article, which forms part of a larger research program is concerned with a static study focussing on the thermo-mechanical system found in the roll gap. This program is aimed at predicting more accurate rolling forces and torques for a hot rolling process [35, 36] as well as the mechanical properties of the strip, by modelling the microstructural evolution of the material by computing the austenite grain size of the strip during hot rolling [11]. The modelling of the microstructural evolution in the roll gap is not the main focus of this dissertation, where the only requirement is to predict the rolling force. Orowan's model has been tried and tested and adhere to the stated requirement, and is thus adequate for use in this dissertation.

The rolling load is a function of the material yield stress (k), rolling geometry and the applied tensions to the strip. The material yield stress is a function of the type of material being rolled, its temperature, the thickness reduction (draft) and the rolling speed. These variables are defined in the sections that follow together with the derivation and adaption of Orowan's model for use in the simulator. Next Orowan's roll gap model will be derived and discussed.

3.3.2 Orowan's differential equation derivation

Table 3.1: Definition of variables for the Orowan model.

Symbol	Definition
$\mu =$	friction coefficient (no dimension)
$s =$	normal roll pressure along the arc of contact (Pa)
$f =$	horizontal force in the roll gap (N)
$p =$	vertical pressure in the roll gap (Pa)
$h_1 =$	sheet centerline thickness at the entrance of the roll gap (m)
$h_2 =$	sheet centerline thickness at the exit of the roll gap (m)
$k(\epsilon, \dot{\epsilon}, \theta) =$	yield stress of the material being rolled (Pa)
$\epsilon =$	strain ($\frac{m}{m}$)
$\dot{\epsilon} =$	strain rate (s^{-1})
$v_{roll} =$	rolling velocity ($m.s^{-1}$)
$R =$	roll radius (m)
$R' =$	deformed roll radius (m)
$\sigma_1 =$	tension stress in the strip at the entrance of the roll gap (Pa)
$\sigma_2 =$	tension stress in the strip at the exit of the roll gap (Pa)
$x_{rg} =$	x coordinate, with the origin at the exit of the roll gap (+ direction against rolling direction) (m)
$\phi_m =$	bite angle (rad)
$\phi =$	angle of arc of contact, measured from the exit of the roll gap (rad)
$\overline{\sigma}(\epsilon, \dot{\epsilon}, \theta) =$	mean flow stress in the roll gap (Pa)
$\theta =$	temperature (°C)
$P' =$	specific rolling force, taking the deformed roll radius into account ($\frac{N}{m}$)
$L_p =$	length of the arc of contact (m)
$S_{arc} =$	arc length of the arc of contact (m)
$\delta = h_1 - h_2$	draft, thickness reduction across the roll gap (m)

Orowan's theory for the calculation of the specific rolling force is implemented [28, 49] in this dissertation. The static model prediction of the specific rolling force is influenced by the strip temperature, roll radius and the deformed roll radius, rolling speed, the material being rolled and the applied tensions.

Orowan's differential equations for the vertical roll pressure and the horizontal roll force in the roll gap will be derived referring to figure 3.2 and table 3.1, where all the necessary variables are defined. The first step in the derivation of the model is to equate the horizontal force balance on the roll gap

element. This force balance is as follows:

$$f(x_{rg}) - f(x_{rg} + dx_{rg}) + 2s(x_{rg})sin\phi\frac{dx}{cos\phi} \pm 2\mu s(x_{rg})cos\phi\frac{dx_{rg}}{cos\phi} = 0, \tag{3.1}$$

note that the top and bottom signs of the double signs ($\pm$ and $\mp$), in Eq. 3.1 and the rest of this derivation, is applicable to the entrance and the exit of the roll gap respectively. The first two terms on the left hand side of Eq. 3.1 can be expressed as,

$$f(x_{rg}) - f(x_{rg} + dx_{rg}) = \frac{-df(x_{rg})}{dx_{rg}}dx_{rg}. \tag{3.2}$$

Substituting the latter into Eq. 3.1 it follows that,

$$\frac{df(x_{rg})}{dx_{rg}} = 2s(x_{rg})\left[tan\phi \pm \mu\right]. \tag{3.3}$$

The horizontal coordinate can be approximated as follows,

$$x_{rg} \approx R'sin\phi. \tag{3.4}$$

Differentiating Eq. 3.4 gives,

$$dx_{rg} = R'cos\phi d\phi. \tag{3.5}$$

If Eq. 3.5 is substituted into Eq. 3.3 the derivative of the horizontal force along the arc of contact can be found,

$$\frac{df(\phi)}{d\phi} = 2R's(\phi)\left[sin\phi \pm \mu cos\phi\right]. \tag{3.6}$$

Equating a vertical force balance on the element of length dx delivers,

$$p(\phi)dx_{rg} = s(x)cos\phi\frac{dx_{rg}}{cos\phi} \mp \mu s(\phi)sin\phi\frac{dx_{rg}}{cos\phi}. \tag{3.7}$$

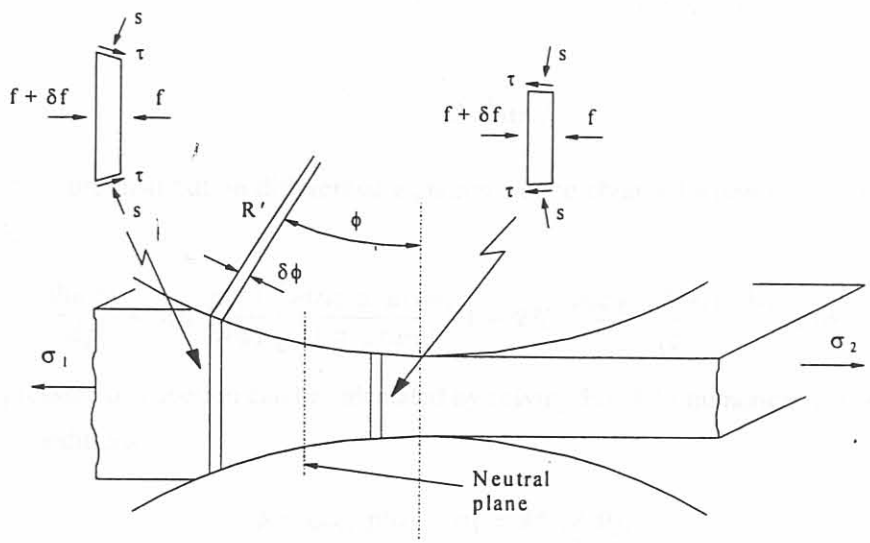

Figure 3.2: Forces acting upon the roll gap element (figure adapted from [1]).

Simplifying Eq. 3.7, the vertical roll pressure as a function of the arc of contact can be obtained,

$$p(\phi) = s(\phi)\left[1 \mp \mu tan\phi\right]. \tag{3.8}$$

Orowan [28] implemented the Huber-Mises yield criterion [24] to account for the plastic deformation in the roll gap. The resulting relation between the vertical roll pressure, horizontal force and yield stress is,

$$p(\phi) - \frac{f(\phi)}{h(\phi)} = k(\epsilon, \dot{\epsilon}, \theta). \tag{3.9}$$

If Eq. 3.8 and Eq. 3.9 are substituted into Eq. 3.6, Orowan's differential equation is obtained,

$$\frac{df(\phi)}{d\phi} = 2R'\left[\frac{f(\phi)}{h(\phi)} + k(\epsilon, \dot{\epsilon}, \theta)\right]\left[\frac{sin\phi \pm \mu cos\phi}{1 \mp \mu tan\phi}\right]. \tag{3.10}$$

The horizontal rolling force, $f(\phi)$, can be used to calculate the specific rolling force (P'), which is a function of the vertical roll pressure. Eq. 3.10 can be manipulated to express the derivative of the vertical roll pressure along the arc of contact.

Defining the spatial coordinate origin at the exit of the roll gap (ϕ and x increases against the rolling direction). The thickness of the sheet at any point in the roll gap can be expressed as:

$$h(\phi) = h_2 + 2R'(1 - cos\phi). \tag{3.11}$$

The Huber-Mises yield criterion (Eq. 3.9) can also be written as,

$$f(\phi) = h(\phi)\left[p(\phi) - k(\epsilon, \dot{\epsilon}, \theta)\right]. \tag{3.12}$$

Differentiating Eq. 3.12 and Eq. 3.11 it follows that,

$$\frac{dh(\phi)}{d\phi}\left[p(\phi) - k\right] + h(\phi)\frac{dp(\phi)}{d\phi} = 2R'p(\phi)\frac{(sin\phi \pm \mu cos\phi)}{(1 \mp \mu tan\phi)}, \tag{3.13}$$

$$\frac{dh(\phi)}{d\phi} = 2R'sin\phi. \tag{3.14}$$

The vertical pressure distribution differential equation can be obtained when Eq. 3.14 is substituted into Eq. 3.13,

$$\frac{dp(\phi)}{d\phi} = 2R'\frac{p(\phi)}{h(\phi)}\left[\frac{sin\phi \pm \mu cos\phi}{1 \mp \mu tan\phi}\right] - 2R'\frac{(p(\phi) - k(\epsilon, \dot{\epsilon}, \theta))}{h(\phi)}sin\phi. \tag{3.15}$$

The vertical pressure distribution can be calculated by solving Eq. 3.15 numerically using the following boundary conditions:

$$\phi = \phi_m,\ p(0) + \sigma_1 = k(\epsilon, \dot{\epsilon}, \theta); \tag{3.16}$$

$$\phi = 0,\ p(\phi_m) + \sigma_2 = k(\epsilon, \dot{\epsilon}, \theta). \tag{3.17}$$

When the vertical pressure distribution is integrated over the arc of contact, the specific rolling force per unit width can be calculated as follows:

$$P' = R' \int_0^{\phi_m} p(\phi) d\phi. \tag{3.18}$$

Assuming that ϕ is small, $1 - cos\phi$ can be substituted with its approximation ($\frac{\phi^2}{2}$) [2, 24], and Eq. 3.11 can be rewritten as,

$$h(\phi) = h_2 + R'\phi^2. \tag{3.19}$$

The arc of contact can then be calculated as,

$$\phi_m = \sqrt{\frac{h(\phi_m) - h_2}{R'}} = \sqrt{\frac{\delta}{R'}}, \tag{3.20}$$

and the horizontal length of the arc of contact is approximated as the arc length,

$$L_p = S_{arc} = R'\phi_m = \sqrt{\delta R'}. \tag{3.21}$$

3.3.3 Roll gap variables

In the previous section and table 3.1 the roll gap variables are listed without a proper description of their characteristics and their influences on the solution methodology of the differential equation model. These variables are mainly functions of temperature, material properties and the draft taken.

3.3.3.1 Deformed roll radius

The vertical rolling pressure causes the work roll to flatten along the arc of contact. For hot rolling processes this flattened arc can be modelled as a larger circular radius with a shifted center [44, 46, 3]. This assumption however might not hold for cold thin strip rolling, temper rolling and foil rolling where the modelling of the roll gap can consist of an alternating combination of five elastic and plastic deformation regions [45, 49].

The specific rolling force, P', is however dependent on the deformed roll radius, R', and the deformed roll radius is again dependent on the specific rolling force associated with the deformed roll radius. This implicit relationship necessitates an iterative solution process in order to solve for the specific rolling force and the deformed roll radius.

The flattened arc radius is calculated using Hitchcock's formula [44, 28]:

$$R' = R\left[1 + \frac{16(1-\nu^2)P'}{\pi E \delta}\right], \tag{3.22}$$

where ν is Poisson's ratio for steel (0.3) [2] and E is Young's modulus of the work rolls.

Elastic recovery of the strip [28, 3] changes the roll gap behaviour. At the entrance and exit of the roll gap there are regions where the strip does not deform plastically but rather elastically, due to higher values of yield stress at these points. The effect of this strip elastic recovery is that the exit thickness of the roll gap is not the final strip thickness and the strip recovers over some small distance to its final thickness. The final sheet thickness is greater than the compressed exit thickness from the roll gap. At the entrance of the roll gap the entrance thickness is elastically compressed before plastic deformation occurs.

Modifying Orowan's differential equation model (Eq. 3.15) by substituting an elastic relationship, instead of the Huber-Mises plastic yielding relationship (Eq. 3.9), into Eq. 3.10 the same differential equation model can be used to solve for the elastic recovery regions of the roll gap. For hot rolling, these elastic recovery effects are negligible and can be omitted from the simulator without loss of generality [3].

3.3.3.2 Friction Coefficient

In the case of hot rolling the friction coefficients at the work rolls and strip interfaces generally fall in the following range: $0.25 \leq \mu \leq 0.45$. A lubricated roll gap exhibits smaller friction coefficients ($0.25 \leq \mu \leq 0.31$) whilst in unlubricated cases the coefficients are between 0.31 and 0.45 [45, 34, 36, 49]. In this work the friction coefficient was taken as a linear function of the roll gap temperature, θ, as follows [50]:

$$\mu(\theta) = 4.86 \times 10^{-4}\theta - 0.0714. \tag{3.23}$$

The friction coefficients of the mill simulator over the temperature range under investigation are,

$$0.342|_{\theta=850^\circ C} \leq \mu(\theta) \leq 0.405|_{\theta=980^\circ C}, \tag{3.24}$$

which correspond to the unlubricated cases.

3.3.3.3 Yield stress model

The material characteristics of the strip are taken into account in this model. Different relationships can be used to describe the flow stress of the metal in the roll gap. Yield stress criterions, such as the Tresca, von-Mises and the Huber-Mises, relate the flow stress to the yield stress [47, 48, 24]. One such flow stress relationship is the Zener-Holoman equation, which describes the relationship between the mean flow stress ($\overline{\sigma}$), mean strain ($\overline{\epsilon}$) and the mean strain rate ($\dot{\overline{\epsilon}}$) which the material is subjected to in the roll gap [2]. This relationship (based on Arrhenius's law) takes the work hardening of the strip and the strain rate sensitivity of the material [34, 2, 24] into account as follows,

$$\overline{\sigma} = A\overline{\epsilon}^{n}\dot{\overline{\epsilon}}^{m} exp(\frac{Q}{R_{ideal}\theta}), \tag{3.25}$$

with,

Q: the activation energy for onset of plastic deformation;

m: the strain rate sensitivity exponent;

n: the work hardening exponent;

R_{ideal}: the ideal gas constant.

The mean strain rate can be calculated by taking the mean strain and dividing it by the time it takes for the material to travel through the roll gap,

$$\dot{\overline{\epsilon}} = \frac{\overline{\epsilon} v_{roll}}{L_p} = \frac{ln\left(\frac{h_1}{h_2}\right) v_{roll}}{\sqrt{R'\delta}}. \tag{3.26}$$

If an appropriate yield criterion is used the yield stress of the material can be calculated from the flow stress across the roll gap [24, 2]. The von-Mises yield criterion defines the mean flow stress as,

$$\overline{\sigma}(\epsilon, \dot{\epsilon}, \theta) = \frac{\sqrt{3}k(\epsilon, \dot{\epsilon}, \theta)}{2}. \tag{3.27}$$

Another approach is to use an equation that relates the yield stress to the roll gap geometry and the temperature in the roll gap as follows:

$$k(\epsilon, \dot{\epsilon}, \theta) = k_{fo} exp^{-k_f \theta} \left(\frac{v}{\sqrt{R'h_1}} \sqrt{\frac{h_1 - h_2}{h_1}} ln\left(\frac{h_1}{h_2}\right) \right)^{k_{fspeed}}, \tag{3.28}$$

where k_{fo}, k_f and k_{fspeed} are model coefficients. This equation was found to yield satisfactory results compared to real plant data[1]. If Eq. 3.28 is investigated there are a few differences from the Zener-Holoman relationship but the similarities outnumber the former. The term $ln\left(\frac{h_1}{h_2}\right)$ represents the mean material strain and $\frac{v}{\sqrt{R'h_1}}$ has a time rate unit representing the mean strain rate. The biggest difference is the different expressions used to calculate the power of the exponential in Eq. 3.25 and Eq. 3.28. In Eq. 3.28 the power expression reflects a linearization, of the hyperbole function in Eq. 3.25, over the temperature range under investigation.

3.4 Tension Model

3.4.1 Introduction

The pieces of strip between the coiler furnaces and the roll gap are continuous distributed parameter mass elements and the theory of continuous dynamics can be employed to model the tensions in the

[1]Eq. 3.28 is used by a large stainless steel manufacturer in South Africa for their setup calculations. The values of the model coefficients are given in chapter 4.

strip. The reason for modelling the tension is to get accurate values of the tension at the entrance and exit of the roll gap. Tension-stresses, $\sigma_1(t), \sigma_2(t)$, decrease the rolling load as can be seen in Eqs. 3.16 and 3.17. In this dissertation it is proposed that tension modelling can be done by approximating the pieces of strip between the coiler furnaces and the roll gap as longitudinal bars that are subjected to longitudinal vibrations [51, 52, 53, 54].

The pieces of strip are however also subjected to transverse vibration. The lateral and longitudinal vibrations of the strip can be viewed separately and their results superimposed on each other, or it can be viewed as a continuous system where the two PDE's have to be solved simultaneously.

There are two possible ways of modelling the transverse vibration of the strip:

1. **Transverse Vibration Strip Model 1:** The strip can be modelled as a bar or beam exhibiting lateral vibration with an axial force applied to the bar or beam [51]. The axial force will typically be the horizontal force ($f(x)$ see figure 3.2) found from the roll gap analysis. The theory used for this model is usually applied to the study of vibration of cables and guy wires [51].

2. **Transverse Vibration Strip Model 2:** The strip can be modelled as a string exhibiting free transverse vibration [54].

A distributed parameter system that vibrates transversely has two sources that act as restoring forces to bring the system to its equilibrium point. These two sources are the axial tension and the bending stiffness [54]. The bending stiffness of the system is the dominant restoring force for the Transverse Vibration Strip Model 1. It can be argued that this model can be reduced to a beam model without the applied axial force; the result being a normal transverse vibration model of a beam, where the solution of this model will give the transverse translation of the system. The strip is however in a temperature range were plastic deformation can easily take place, and it can be argued that the strip will not exhibit meaningful bending stiffness. The strip can thus not be modelled as a bar or beam subjected to transverse vibration.

For Transverse Vibration Strip Model 2 the axial tension is the dominant restoring force. It is debatable whether the second model will give a more accurate reflection of the transverse vibration of the sheet outside the roll gap. With the second model the lateral and transverse vibration problems can be combined and the mutual influences on each other, for the rolling mill application, can be accounted for as follows:

- The longitudinal vibration of the strip, for both sides of the roll gap, can be modelled as a uniform bar, for which the longitudinal vibration is given as follows,

$$E_{ss}A\frac{\partial^2 u}{\partial x^2}(x,t) \pm f(x,t) = \rho A\frac{\partial^2 u}{\partial t^2}(x,t). \tag{3.29}$$

- The tension force in the strip, when modelled as a bar, can be expressed as,

$$T(x) = E_{ss}A\frac{\partial u}{\partial x}(x,t). \tag{3.30}$$

- Eq. 3.30 can then be substituted into the PDE describing the transverse vibration of a string,

$$\frac{\partial}{\partial x}\left[T(x)\frac{\partial y}{\partial x}(x,t)\right] = \rho A\frac{\partial^2 y(x,t)}{\partial t^2}, \tag{3.31}$$

where,

E_{ss}: Young's modulus of the strip;

A: Cross sectional area perpendicular to the rolling direction;

ρ: Density of the strip metal;

x: Rolling direction;

$u(x,t)$: Lateral displacement of the strip metal;

$y(x,t)$: Transverse displacement of the strip metal;

$T(x)$: Tension in the sheet as a function of the rolling direction expressed as a force;

$f(x,t)$: Horizontal force per unit width found from the roll gap analysis[2].

It should be stressed that the transverse vibration will not be symmetrical for the physical system due to the roller table that will limit downward transverse displacement.

Since only the tension into the roll gap and tension just outside the roll gap need to be known for solving Orowan's static differential equations, in depth modelling of the tension of the sheet is not necessary for this investigation. However, if the simulator's capability is to be increased to account for shape formation and the residual stress build-up in the sheet, it will be necessary to account for the non-uniform elongation of the strip along the length and across the width of the strip. The suggested modelling approach might be worthwhile investigating to create a simulator that can account for the stress and strain of the strip at different points on the strip.

For the purpose of this dissertation it is sufficient to model the tension behaviour of the strip (in the mill simulator) as discrete springs in tension [55, 56], as will be described in the following section.

3.4.2 Tension Model

In practice, a certain tension is required in the strip in order to reap the benefit of a reduced rolling load. This required tension is determined by a setup program that calculates all the mill parameters

[2] $+f(x,t)$: Strip piece from back coiler to the entrance of the roll gap.

$-f(x,t)$: Strip piece from the roll gap exit to the front coiler.

before rolling commences, as is discussed in section 2.3. The tension in the strip is perturbed around this required tension because of factors such as roll gap thickness adjustments[3]. If the rolling load can be reduced, the draft taken off the strip can be increased without violating the physical constraint on the total rolling force (40 MN) for the Steckel Mill under consideration. Thus, the main control aim is to regulate the tension in the sheet around the setup tension value.

It is assumed that the base tension is established before the mill drive is accelerated towards the threading speed for the particular pass. At threading speed the coiler motors' speeds are controlled in such a manner that the tangential speed of the strip at the front/back coiler drum remains approximately the same as the exit/entrance speed of the roll gap respectively. The radiuses of the front and back coils are increasing and decreasing respectively with time. In order to keep the tangential strip speeds constant, the angular velocities of the coiler motors have to be controlled according to the relationship, $\omega_{coiler\ drive} = \frac{v_{tangential}}{R_{coil}}$.

If a mismatch in coiler speeds and roll gap speeds should occur, the strip tension increases or decreases depending on the change in speeds and on which side of the roll gap this change occurs. The strip reflects these changes by stretching more or less respectively. It is not desirable that the strip should break due to necking[4] or vibrate transversely (perpendicular to the rolling direction) due to the relaxation of tension[5]. In order to model this phenomena it was decided to model the strip pieces from the roll gap to the coilers as discrete springs already under tension. The setup values for the applied tensions are calculated using the following[6],

$$T_i = 47wh_i^{0.27}, \forall i \in [1,2], \tag{3.32}$$

where T_i is expressed in Newtons and w, h_i are both expressed in millimeter.

The tension model can be expressed as follows [55, 56]:

$$T_1 = \frac{E_{ss}(h_1 w_{strip})}{L_{cf\leftrightarrow rg}} \int_0^t (v_1(\tau) - v_{bc}(\tau))\, d\tau \tag{3.33}$$

$$T_2 = \frac{E_{ss}(h_2 w_{strip})}{L_{cf\leftrightarrow rg}} \int_0^t (v_{fc}(\tau) - v_2(\tau))\, d\tau \tag{3.34}$$

with,

[3]When the roll gap distance is changed, the draft of the strip varies, changing the entrance and exit speed of the roll gap. These speed changes cause the tension to vary according to Eqs. 3.33 and 3.34.

[4]Necking occurs when the strip deforms plastically (the tension stress in the strip is larger than the strip's yield stress) outside the roll gap, resulting in an observable thickness reduction and a less observable width reduction.

[5]In this instance tension can be seen as negative and the effect of applied tension to the roll gap model should be zero.

[6]This setup equation for the tension is used by a large stainless steel manufacturing company in South Africa for their tension setup calculations.

T_1: Tension in the strip piece from the back coiler to the roll gap (expressed in N);

T_2: Tension in the strip piece from the roll gap to the front coiler (expressed in N);

E_{ss}: Young's modulus for Stainless Steel Grade 304 (Pa);

w_{strip}: Strip width (m);

v_{fc}: Tangential velocity of the strip taken up on the front coiler (m/s);

v_{bc}: Tangential velocity of the strip paid off by the back coiler (m/s);

$L_{cf\leftrightarrow rg}$: The length from the coiler furnaces to the roll gap (ignoring the length of the arc of contact[7], m).

3.5 Stand Model

3.5.1 Introduction

The stand model derived in this section is unique and more comprehensive than stand models found in the literature [7, 40]. There are some similarities between the stand model derived in this section and the models depicted in [7, 40]. The distinctions and similarities of the stand model and the models in [7, 40] will be highlighted during the following discussion and model derivation.

The model is divided into a continuous mass system (4 rolls) interacting with discrete elements (lumped masses and springs) as depicted in figure 3.3. The lumped masses are formed by lumping the roll chock and bearing combinations together, resulting in eight discrete masses. Although it can be argued that the system exhibits symmetry properties, it was however decided not to make symmetry approximations, setting this model apart from models in [7, 40].

This modelling choice can be motivated by referring to the practical behaviour of the rolling stand [40, 27, 7]. Shearing forces at the end points of the rollers interact with the discrete modelled masses and springs, representing the roll chocks and bearings, as well as with hydraulic actuators and jacks. The top back-up roll chocks are connected to hydraulic actuators keeping the top back-up roll at the desired setting. The hydraulic actuator is mounted in the mill frame. The rolling force is transmitted to the mill frame from the roller end points to the hydraulic actuator and then to the mill frame. The rolling mill stand does not exhibit infinite stiffness and the large rolling forces, necessary to achieve the plastic deformation of the strip, cause the rolling mill frame to stretch. This stretch is asymmetrical and in an upwards direction, when the base of the rolling mill frame is chosen as the reference point. This stretch is also asymmetrical around the mill's width centerline, due to different mill springs for

[7]The length of the arc of contact is 50 mm and $L_{cf\leftrightarrow rg}$ is approximately 6.4m. The first value was obtained from simulation of the roll gap model as discussed in chapter 4 and 5. The second value was calculated from data obtained from a questionnaire about the Steckel mill under investigation.

the **D**rive and **O**perator **S**ides (DS and OS) of the rolling mill.

The action and reaction forces in the roll gap push the working rolls apart while at the same time also bending them. The width of the mill stand is larger than the width of the strip. If mill stretch is neglected the setup of the roll gap position is kept constant at the end points of the top back-up roll. The relative displacements of the rollers at their end points deviate slightly, but the objective is to keep them fixed by controlling the hydraulic stroke. The rollers deform elastically by bending along their axes in order to cope with the large rolling forces on the strip/work roll interfaces.

The rollers are designed to be very rigid and limit the amount of bending of the rolls along their axis. The stiffness of a roller decreases as the diameter of the roll decreases and the roller is bended more easily. Back up rollers are normally used to limit the amount of bending of the thinner work rolls. In order to roll thinner gauges smaller diameter work rolls are used [57]. From the preceding discussion it is evident that these small diameter rolls will easily bend and the need for other larger diameter rollers, to decrease the amount of bending of the working rolls, arise. There is thus a tradeoff between the diameter of the work rolls and the amount of allowed bending. The Z-high mill and the Sendzimer cold rolling mills serve as examples, where the rolling of thinner gauges, with small diameter work rolls and a number of supporting rolls.

3.5.2 Literature review

Different methods have been developed to predict the strip thickness profile and shape. These can be divided into the following groups [10, 17, 58]:

- Elastic Foundation Method
- Influence Coefficient Method
- Slit Beam Models
- Finite Element Method (FEM)
- Spring and Beam Method
- Transport matrix Method

The modelling approach decided upon was the elastic foundation method although in [10, 17, 58] it is suggested that this type of modelling is inferior to some of the other models. These limitations to simple beam models are given in the literature as follows:

- **Remark 1:** Usually static bending models [10] are obtained from this method and are not suitable for mill setup and on-line control due to their limited application and are used for

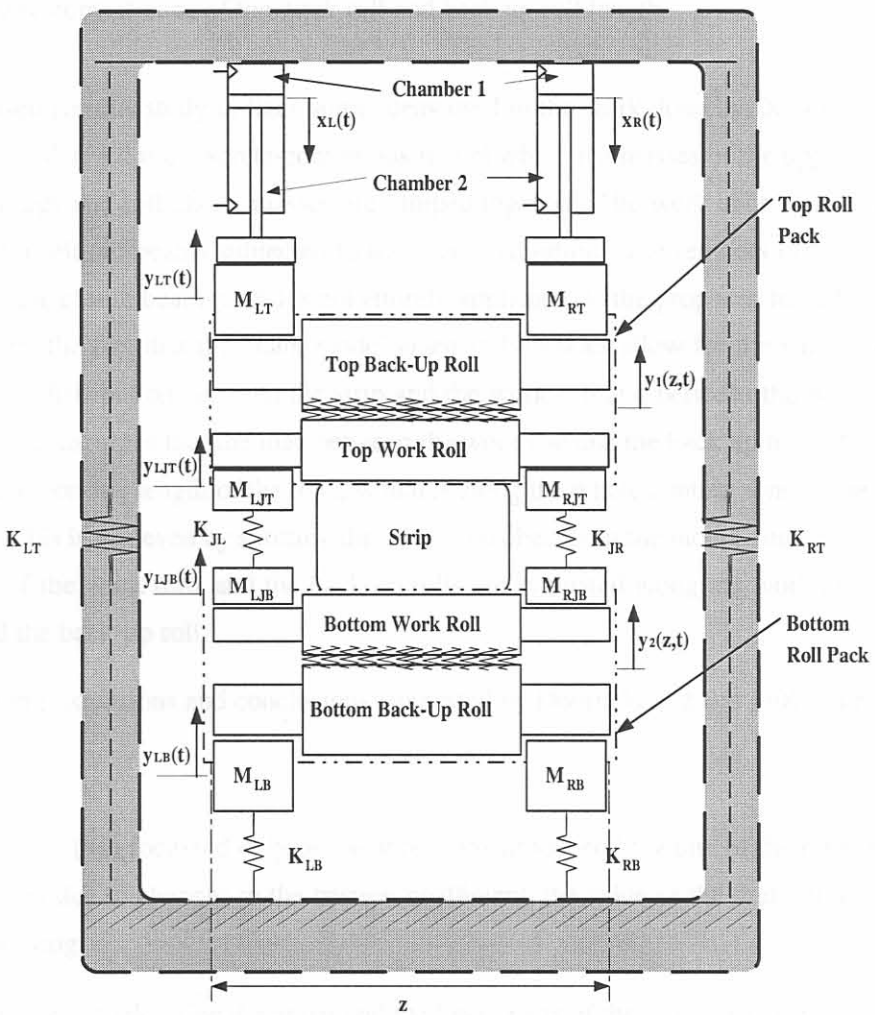

Figure 3.3: Cross sectional view of the mill stand and the hydraulic cylinders.

approximate estimations of control devices during the mill design stage [17, 58]. However, in [59] this type of modelling approach was successfully used for the design of an observer and a MIMO controller.

- **Remark 2:** The simple beam models given in [10] do not allow for the simulation of uneven transverse load distributions between the strip and the work roll and between the work roll and back-up roll. Furthermore it is assumed that the load between the work roll and the back up roll is transmitted only along the strip width, which contradicts the actual loading, which is along the whole contact zone of the work roll and back up roll length.

The model used for this study utilizes some ideas used in the work done by Dobrucki and Bar [40]. The model they derived is a discrete-continuous model where the masses of the upper part of the mill housing, bearings and roll chock masses are lumped together. The work rolls and the back-up rolls are modelled as elastic beams subjected to transverse vibration. The remarks of various authors on the quality of the elastic beam model is not entirely applicable to the proposed model. This statement is motivated by the fact that the beam model given in [40] does allow for the simulation of uneven transverse load distribution between the strip and the work roll and between the work roll and back up roll. It further assumes that the load between the work roll and the back up roll is transmitted only along the axial working length of the rolls, which is along the whole contact zone of the work roll and back up roll. This is achieved by splitting the continuous beams of the model, into five smaller beams. The loading of the work rolls and the back-up rolls are evaluated along the working axial length of the work and the back-up roll.

Some modelling extensions and conclusions suggested by Dobrucki and Bar [40] can be described as follows:

- Their study [40] focussed only on the vibrations produced by a bite of the rolls, neglecting the vibrations due to changes in the friction coefficient, the value of the draft, and the phenomena of chattering.
- They propose to describe the upper and the lower parts of the stand in an asymmetrical fashion.
- They found that there was a discrepancy between their model and the real plant data used to test their model. It was found that the periods and the amplitudes of the vibrations of the rolls, on the mill drive side, is greater than on the operator side. Thus the model has to be asymmetric, with respect to the mass of the spindles. This phenomenon can be attributed to the chattering (torsional vibration of the mill drive spindles) of the mill, as well as the difference in the mill spring of the mill frame on both sides of the mill.

In this dissertation some of the modelling extensions proposed by Dobrucki and Bar are taken into account.

- Firstly, the vibration effect due to changing draft and the variation of the friction coefficient with temperature are taken into account in the simulator roll gap model. The specific rolling force interacts on its part with the dynamic stand model and the forced vibration results in a draft deviation, which again influences the calculation of the specific rolling force at the next time step. Thus the vibration due to the varying draft is incorporated in the mill simulator.
- Secondly the upper and lower part of the rolling mill are investigated in an asymmetrical fashion.
- Thirdly in order to account for the asymmetrical behaviour between the DS and OS vertical roller displacements, different mill stretch curves for either side of the mill frame are modelled. The effect of chattering of the mill drive spindles is not taken into account in this dissertation.

3.5.3 Modelling Assumptions

It is assumed that the bending and deflection of the work and back-up rolls can be modelled as beams that interact with each other and with the discrete components. An example on how to construct the PDE model to account for the interaction between discrete model components and a continuous mass beam is shown in [51]. The beam-beam interaction can be modelled as a beam on an elastic foundation [54, 60]. In the following section a more elaborate description of the modelling choices will be given.

In this work a few simplifying assumptions are made that is in accordance with assumptions made in [40, 59, 61]):

- The second moment of area is taken as a constant and the bending of the beam does not influence the second moment of area appreciably along the length of the roll, z;
- Time varying effects that increase/decrease the radiuses of the rollers, such as thermal crown build-up and deformed roll radiuses on the strip/roll and roll/roll interfaces are assumed negligible. Thus the cross-sectional area of the rolls do not change along the length of the rolls (z) due to these varying effects and only changes due to the different radiuses for the working interface of the roll and the roll necks;
- Poisson deformation of the rollers along the width of the rollers is negligible.

3.5.4 Partial Differential Equation (PDE) Model

The basic PDE for an unforced elastic beam is given as [51, 54, 60],

$$\rho A(z)\frac{\partial^2}{\partial t^2}y(z,t) + \frac{\partial^2}{\partial z^2}\left[EI(z)\frac{\partial^2}{\partial z^2}y(z,t)\right] = 0. \tag{3.35}$$

The beam's second moment of area (taking the simplifying assumptions into consideration) can be expressed as follows:

$$I_i(z) = \begin{cases} I_{i1} = \frac{\pi(2r_{neck_{is}})^4}{64}, \forall -\frac{l_i}{2} \leq z < -\frac{w}{2}, \in z_1 \\ I_{i2} = \frac{\pi(2r_{work_i})^4}{64}, \forall -\frac{w}{2} \leq z \leq \frac{w}{2}, \in z_2 \\ I_{i3} = \frac{\pi(2r_{neck_{is}})^4}{64}, \forall \frac{w}{2} < z \leq \frac{l_i}{2}, \in z_3 \end{cases}, \tag{3.36}$$

where $i \in [1,2,3,4]$ is the index of the rollers, $s \in [L,R]$ is the index reflecting the side of the mill under consideration, l_i is the length of the roller and w is the width of the strip. The domains z_1, z_2 and z_3 can be described as follows (Assuming an uneven pass is executed):

z_1: Length of the roller from its left end (OS) point to the working roll surface;

z_2: Length of the roller's working surface;

z_3: Length of the roller from the end of the working surface, right of the mill centerline (DS), to the end of the roller.

Similarly the cross sectional areas of the rollers are expressed as:

$$A_i(z) = \begin{cases} A_{i1} = \pi r^2_{neck_{is}}, \forall z \in z_1 \\ A_{i2} = \pi r^2_{work_i}, \forall z \in z_2 \\ A_{i3} = \pi r^2_{neck_{is}}, \forall z \in z_3 \end{cases}. \tag{3.37}$$

From Eq. 3.36 it is evident that although $I_i(z)$ is an implicit function of z and the second derivative, $\left(\frac{\partial^2}{\partial z^2} EI(z)\right) \cdot \frac{\partial^2}{\partial z^2} y(z,t) = 0$, and Eq. 3.35 can be simplified to yield,

$$\rho A(z) \frac{\partial^2}{\partial t^2} y(z,t) + EI(z) \frac{\partial^4}{\partial z^4} y(z,t) = 0. \tag{3.38}$$

The work rolls and the back-up rolls interact with each other. On the interfaces between the back-up rolls and work rolls, the rolls can be compressed if the relative movement of the rolls are such that:

- The vertical displacement of the top back-up roll is less than the vertical displacement of the top work roll.
- The vertical displacement of the bottom work roll is less that the vertical displacement of the bottom back up roll.

When the rolls are compressed at the roll interfaces the equation for the value of the spring coefficient is given by Stone in [62]. The decrease in compressive distance between the centers of the two contacting rolls is given as:

$$\triangle = \frac{P'}{E} \frac{2(1-\nu^2)}{\pi} \left[\frac{2}{3} + ln\frac{2D_1}{b} + ln\frac{2D_2}{b}\right], \tag{3.39}$$

where:

P': Specific rolling force;

υ: Poisson's ratio for steel;

E: Young's modulus of the rollers (steel) ;

D_1, D_2: diameters of the rolls under compression;

$\triangle$: Compressive distance between the back-up and work roll interface.

The width of the flattened contact area of the roller interface along the axial length of the rollers is given as,

$$b = \sqrt{\frac{16(1-\nu^2)}{\pi}\frac{P'}{E}\frac{D_1 D_2}{D_1 + D_2}}. \tag{3.40}$$

With $\triangle$ known the distributed spring constant (units: $\frac{N/m}{m}$) can be calculated as,

$$k_{interface}(P') = \frac{P'}{\triangle}. \tag{3.41}$$

Due to the bending of the rolls over the width of the mill, different draft values are obtained over the width of the strip, resulting in varying specific rolling force along the width of the rolls. The varying specific rolling force results in a varying interface loading spring constant along the width of the compressed rolls.

Taking the above and the relative movement conditions into consideration, the compression of the rolls can be modelled as a nonlinear distributed spring system expressed as,

$$k_{c_j}(P'(z,t),z) = \begin{cases} k_{interface}(P'),\ y_i(z,t) \leq y_{i+1}(z,t) \\ 0,\ for\ y_i(z,t) > y_{i+1}(z,t) \end{cases}, \tag{3.42}$$

where $i \in [1,3]$ and $j \in [1 \leftrightarrow 2, 3 \leftrightarrow 4]$. In figure 3.3 the directions of the vertical displacements are shown.

3.5.5 Four-High Stand

3.5.5.1 Top Back Up Roll (TBU)

The top back-up roll's adjacent model elements are the discrete lumped masses at each of the TBU ends as well as the top work roll (TWR).

The top back up roll's adjacent model elements are the discrete lumped mass at each of its ends as well as the top work roll.

$$\rho A_1(z)\frac{\partial^2}{\partial t^2}y_1(z,t) + EI_1(z)\frac{\partial^4}{\partial z^4}y_1(z,t) = -k_{c_{1\leftrightarrow 2}}(P'(z,t),z)(y_1(z,t) - y_2(z,t)) \tag{3.43}$$

The Boundary Values of the model are:

$$\frac{\partial}{\partial z}y_1(z,t)\Big|_{z=\frac{-l_1}{2}} = 0 \tag{3.44}$$

$$\frac{\partial}{\partial z}y_1(z,t)\Big|_{z=\frac{l_1}{2}} = 0 \tag{3.45}$$

$$EI_1(z)\frac{\partial^3}{\partial z^3}y_1(z,t)\Big|_{z=\frac{-l_1}{2}} = M_{LT}\ddot{y}_{LT}(t) + F_{HAL} \tag{3.46}$$

$$-EI_1(z)\frac{\partial^3}{\partial z^3}y_1(z,t)\Big|_{z=\frac{l_1}{2}} = M_{RT}\ddot{y}_{RT}(t) + F_{HAR} \tag{3.47}$$

These boundary values are in accordance with the modelling work of Pederson [7, 59]. The boundary values for all four rollers have the same structure and their physical meaning can be described as follows:

- $\frac{\partial}{\partial z}y_i(z,t)\Big|_{z=\frac{-l_i}{2},\frac{l_i}{2}}$, $\forall i \in [1,2,3,4]$: The rollers are encapsulated in the roll neck and bearing capsule. The rolls are not able to bend in such a way that the slope of the rollers at the end of the rollers are non zero.
- $\frac{\partial^3}{\partial z^3}y_i(z,t)\Big|_{z=\frac{-l_i}{2},\frac{l_i}{2}}$, $\forall i \in [1,2,3,4]$: The shearing forces of the rolls are non-zero and interact with the discrete parts of the model.

The modelling work of Dobrucki and Bar [40] further differ from the approach given in this dissertation, than already highlighted. Dobrucki and Bar did not take the boundary condition into account that arises due to the encapsulation of the roller. They also divided each roller into five distinct beams, as was earlier remarked. Three beams were used to account for the rollers working interface and the remaining beams were used to account for the roll necks. The three beam elements that model the working interface of a roller are in contact with the adjacent roller's three beam elements. The middle beam of the work roll is the only beam that is in contact with the strip. In this dissertation it was decided to look at a roller as one beam with different radiuses for the roll necks and the working surface.

3.5.5.2 Top Work Roll (TWR)

The top work roll's adjacent model elements are the TBU, the strip and discrete elements, i.e. the bearings, roll chocks and the hydraulic jack actuator.

$$\rho A_2(z)\frac{\partial^2}{\partial t^2}y_2(z,t) + EI_2(z)\frac{\partial^4}{\partial z^4}y_2(z,t) = P'(z,t) + k_{c_{1\leftrightarrow 2}}(P'(z,t),z)(y_1(z,t) - y_2(z,t)) - k_{strip}(y_2(z,t) - y_3(z,t)) - \beta_{strip}(\dot{y}_2(z,t) - \dot{y}_3(z,t)) \quad (3.48)$$

Boundary Values:

$$\frac{\partial}{\partial z}y_2(z,t)\Big|_{z=\frac{-l_2}{2}} = 0 \quad (3.49)$$

$$\frac{\partial}{\partial z}y_2(z,t)\Big|_{z=\frac{l_2}{2}} = 0 \quad (3.50)$$

$$EI_2(z)\frac{\partial^3}{\partial z^3}y_2(z,t)\Big|_{z=\frac{-l_2}{2}} = K_J(y_2(z,t) - y_3(z,t))\Big|_{z=\frac{-l_2}{2}} - J(t) \quad (3.51)$$

$$EI_2(z)\frac{\partial^3}{\partial z^3}y_2(z,t)\Big|_{z=\frac{l_2}{2}} = -K_J(y_2(z,t) - y_3(z,t))\Big|_{z=\frac{l_2}{2}} + J(t) \quad (3.52)$$

3.5.5.3 Bottom Work Roll (BWR)

The bottom work roll's adjacent elements are the BBU, the strip and the discrete components of the hydraulic jacks and the roll chock and bearing combination.

$$\rho A_3(z)\frac{\partial^2}{\partial t^2}y_3(z,t) + EI_3(z)\frac{\partial^4}{\partial z^4}y_3(z,t) = -P'(z,t) - k_{c_{3\leftrightarrow 4}}(P'(z,t),z)(y_3(z,t) - y_4(z,t)) + k_{strip}(y_2(z,t) - y_3(z,t)) + \beta_{strip}(\dot{y}_2(z,t) - \dot{y}_3(z,t)) \quad (3.53)$$

Boundary Values:

$$\frac{\partial}{\partial z}y_3(z,t)\Big|_{z=\frac{-l_3}{2}} = 0 \quad (3.54)$$

$$\frac{\partial}{\partial z} y_3(z,t)\Big|_{z=\frac{l_3}{2}} = 0 \tag{3.55}$$

$$EI_3(z)\frac{\partial^3}{\partial z^3} y_3(z,t)\Big|_{z=\frac{-l_3}{2}} = -K_J(y_2(z,t) - y_3(z,t))\Big|_{z=\frac{-l_3}{2}} + J(t) \tag{3.56}$$

$$EI_3(z)\frac{\partial^3}{\partial z^3} y_3(z,t)\Big|_{z=\frac{l_3}{2}} = +K_J(y_2(z,t) - y_3(z,t))\Big|_{z=\frac{l_3}{2}} - J(t) \tag{3.57}$$

3.5.5.4 Bottom Back-Up Roll (BBU)

The bottom back-up roll's adjacent model components are the BWR and discrete elements, i.e. the load cells and the roll chock and bearing combinations.

$$\rho A_4(z)\frac{\partial^2}{\partial t^2} y_4(z,t) + EI_4(z)\frac{\partial^4}{\partial z^4} y_4(z,t) = -k_{c_{3\leftrightarrow 4}}(P'(z,t),z)(y_4(z,t) - y_3(z,t)) \tag{3.58}$$

Boundary Values:

$$\frac{\partial}{\partial z} y_4(z,t)\Big|_{z=\frac{-l_4}{2}} = 0 \tag{3.59}$$

$$\frac{\partial}{\partial z} y_4(z,t)\Big|_{z=\frac{l_4}{2}} = 0 \tag{3.60}$$

$$EI_4(z)\frac{\partial^3}{\partial z^3} y_4(z,t)\Big|_{z=\frac{-l_4}{2}} = m_{LB}\ddot{y}_{LB}(t) + K_{LB}y_{LB}(t) \tag{3.61}$$

$$EI_4(z)\frac{\partial^3}{\partial z^3} y_4(z,t)\Big|_{z=\frac{l_4}{2}} = -m_{RB}\ddot{y}_{RB}(t) - K_{RB}y_{RB}(t) \tag{3.62}$$

3.5.6 Two-High stand

The four high stand model can be simplified to yield a two-high stand model. It is obtained by grouping the top work roll and top back-up roll and similarly the bottom work roll and back-up

rolls together to form upper (**TRP**-Top Roll Pack) and lower (**BRP**-Bottom Roll Pack) roll packs. This simplification is in accordance with [59] and similar simplifications are suggested in [10, 40]. Dobrucki and Bar [40] stated that the modes of the vibrations of the back-up and work rolls are close to identical and they proposed that the adjacent work roll and the back-up roll be modelled as a one beam unit, supporting the modelling choice in [59] and this dissertation. In this dissertation the derived four beam model is simplified to yield a two beam model that is implemented in the mill simulator. Reasons for this simplification can be summarized as:

- The number of rolls and their interactions increase the complexity of the model and make it infeasible to simulate with the available computing power. Four p states are associated with each roller, where p is the number of accurate natural spatial vibration modes. The solution methodology followed in order to calculate these natural modes of vibration will be discussed in chapter 4.

- The interface loading between the back-up and work rollers makes the stand model time variant[8] due to the nonlinear spring associated with the interface loading, Eq. 3.42. This time dependency requires the solution of an Eigenvalue problem in an iterative solution scheme at each time step and this considerably complicates the mill simulator. The proposed solution for this model is briefly discussed in chapter 4.

- The simulator developed in this dissertation does not model the roller wear and thermal expansion of the working rolls. These two variables have a direct influence on the strip crown and shape and this influence is larger than the indirect influence of the work/back-up roll interface compression on the strip crown and shape. Following the same reasoning the accuracy of the simulator will not be influenced significantly, by the omission of the interface loading from the simulator modelling. In order to illustrate the comparison between the effects of roller wear and thermal crown on strip crown and shape the reader is referred to figure 5 in [63]. From this it can be concluded that work roll wear plays a larger part in crown evolution when compared to the thermal crown build-up on the rollers. Roller wear is a function of many factors, such as the rolling regime and natural roller crown. In figure 5, [63] the absolute value of the crown amplitude associated with roller wear was twice the amplitude of the thermal crown build-up on the rollers.

- Remark 2 in section 3.5.2 was that a problem associated with the use of the elastic beam method is that the differences in the widths of the strip/work roll interface and the work roll/back-up roll interface are not accounted for and are generally taken to be the same. For the two roll pack model, considered further in this dissertation, the difference between the roll pack width and the strip/roll pack interface width is accounted for.

[8] In state-space format it is expressed as $\dot{\mathbf{x}}(t) = \mathbf{A}(t)\mathbf{x}(t) + \mathbf{B}\mathbf{u}(t)$.

3.5.6.1 Top Roll Pack

The area of the roll pack is the summation of the areas of work roll and back roll. The second moment of area, I, of the roll pack is found by taking the second moment of area of the corresponding work roll [59, 50]. Taking this simplifications into account the 4-high model can be modified to yield the following 2-high model[9]:

$$\rho A_{12}\frac{\partial^2}{\partial t^2}y_{12} + EI_{12}\frac{\partial^4}{\partial z^4}y_{12} = P' - k_{strip}(y_{12} - y_{34}) - \beta_{strip}(\dot{y}_{12} - \dot{y}_{34}), \tag{3.63}$$

where,

y_{12}: Is the vertical displacement of the top roll pack;

y_{34}: Is the vertical displacement of the bottom roll pack;

A_{12} : is the area of the top roll pack. This area is taken as the sum of the areas of the work roll and the back-up roll ($A_{12} = A_1 + A_2$);

I_{12}: is the second moment of area of the top roll pack. Note that the second moment of area of the roll pack is taken as only the second moment of area of the work roll [59] ($I_{12} = I_2$). The definition of all the other variables are left unchanged.

The Boundary Values of the model are:

$$\frac{\partial}{\partial z}y_{12}(z,t)\Big|_{z=\frac{-l_{12}}{2}} = 0\ ; \tag{3.64}$$

$$\frac{\partial}{\partial z}y_{12}(z,t)\Big|_{z=\frac{l_{12}}{2}} = 0\ ; \tag{3.65}$$

$$EI_2\frac{\partial^3}{\partial z^3}y_{12}\Big|_{z=\frac{-l_{12}}{2}} = m_{LT}\ddot{y}_{LT} + K_J(y_{12} - y_{34})\Big|_{z=\frac{-l_{12}}{2}} - J + F_{HAL}; \tag{3.66}$$

$$EI_2\frac{\partial^3}{\partial z^3}y_{12}\Big|_{z=\frac{l_{12}}{2}} = -m_{RT}\ddot{y}_{RT} - K_J(y_{12} - y_{34})\Big|_{z=\frac{l_{12}}{2}} + J - F_{HAR}. \tag{3.67}$$

3.5.6.2 Bottom Roll Pack

$$\rho A_{34}\frac{\partial^2}{\partial t^2}y_{34} + EI_{34}\frac{\partial^4}{\partial z^4}y_{34} = -P' + k_{strip}(y_{12} - y_{34}) + \beta_{strip}(\dot{y}_{12} - \dot{y}_{34}), \tag{3.68}$$

[9]The dependency notation of the variables, A_i, y_i, I_i, P', on z and t are omitted in the following section for the sake of brevity.

where,

A_{34}: Is the area of the top roll pack ($A_{34} = A_3 + A_4$);

I_{34}: is the second moment of area of the top roll pack ($I_{34} = I_3$).

The following boundary conditions apply,

$$\frac{\partial}{\partial z} y_{34}(z,t)\Big|_{z=\frac{-l_{34}}{2}} = 0\ ; \tag{3.69}$$

$$\frac{\partial}{\partial z} y_{34}(z,t)\Big|_{z=\frac{l_{34}}{2}} = 0\ ; \tag{3.70}$$

$$EI_3 \frac{\partial^3}{\partial z^3} y_{34}\Big|_{z=\frac{-l_{34}}{2}} = -K_J(y_{12} - y_{34})\Big|_{z=\frac{-l_{34}}{2}} + J + m_{LB}\ddot{y}_{LB} + K_{LB}y_{LB} \tag{3.71}$$

$$EI_3 \frac{\partial^3}{\partial z^3} y_{34}\Big|_{z=\frac{l_{34}}{2}} = +K_J(y_{12} - y_{34})\Big|_{z=\frac{l_{34}}{2}} - J - m_{RB}\ddot{y}_{RB} - K_{RB}y_{RB} \tag{3.72}$$

The solution methodology used to solve the PDE model for the two roll pack model in order to create the mill simulator will be described in chapter 4.

3.5.7 Gaugemeter Compensation

The mill frame does not exhibit infinite stiffness and stretches significantly due to the rolling forces associated with normal operation. The classical and most employed control scheme used to compensate for the mill stretch is the BISRA-Davy gaugemeter compensator [1, 27]. This compensator uses positive force feedback to control the thickness deviation. There are a few deficiencies of this controller that make it necessary to include an X-Ray feedback or feedforward thickness control loop.

The BISRA-Davy gaugemeter compensator equation is given as [27],

$$\delta h_2 = \delta x + \frac{\delta F}{M}, \tag{3.73}$$

With the variables defined as:

M: Mill modulus;

δx: Deviation in stroke of hydraulic actuator;

δF: Deviation in rolling force;

δh_2: Deviation in strip output thickness from the roll gap.

The basic principle of the BISRA-Davy gaugemeter compensator is to regulate the rolling force and effectively combating the stretch by changing the hydraulic stroke in accordance. If the rolling force

is constant, $\delta F = 0$, the desired reduction can be achieved, $\delta h_2 = 0$, according to the BISRA-Davy gaugemeter compensator equation, Eq. 3.73.

From figure 3.4[10] it can be seen that the mill frame stretches about 5mm on either side of the mill when a total force of 30MN (15MN per side) is measured. Thus the mill stretch can be immense and if uncompensated for, no reduction will take place. The mill stretch is an essential component of the mill dynamics and has to be modelled. From simulations it became apparent that the need for the inclusion of a BISRA-Davy gaugemeter compensator need only be included for initial compensation. The dynamic gaugemeter compensator only adds a trim to the setpoint fed to the hydraulic actuators. The BISRA-Davy gaugemeter compensator were modelled as part of the plant to aid with the maintenance of steady state conditions, before step tests were applied to the plant in order to identify a linear plant using system identification. These trim values will not contribute significantly to the dynamics of the identified model as is discussed in chapter 5. A differential gaugemeter compensator was not implemented and only a mean gaugemeter compensator was modelled.

The mill stretch can be modelled as a two piece function consisting of a nonlinear power function and a linear function. The power, χ, and gain, k_a, of the non linear function can be calculated as,

$$\chi_s = \frac{F_{roll_{test_s}}}{K_{sT} M S_{test_s}}, \tag{3.74}$$

$$k_{a_s} = y_{stretch_{test_s}} F_{roll_{test_s}}^{-\chi_s}, \tag{3.75}$$

respectively, where s is an index indicating which side of the mill is under investigation and $F_{roll_{test_s}}$ is the initial force measured by the load cells with no strip in the roll gap. $y_{stretch_{test_s}}$ is the initial mill stretch that is measured under this initial load and K_{sT} is the extended linear mill spring calculated from data logged when the rolls, in the absence of a strip, are pressed against each other with increasing force steps until a measured force of 15MN per side is registered. Practical values for these parameters will be given in chapter 4. The mill stretch model as a function of the applied force for both sides of the mill frame can be expressed as:

$$y_{stretch_s}(F_{roll_s}) = \begin{cases} k_{a_s} F_{roll_s}^{\chi_s}, \forall 0 \leq F_{roll_s} \leq F_{roll_{test}} \\ \frac{1}{K_{sT}}(F_{roll_s} - F_{roll_{test_s}}) + y_{stretch_{test_s}}, \forall F_{roll_{test_s}} < F_{roll_s} \leq \frac{30MN}{2} \end{cases}, \tag{3.76}$$

where $s \in [L, R]$, F_{roll_s} is the applied force and $y_{stretch_s}$.

From figure 3.4 the mill stretch curves seem to be nearly linear over the operation range. Figure 3.5 emphasizes the asymmetry of the rolling mill frame. The calculated linear mill spring coefficients for both sides of the mill will be given in chapter 4.

[10]Figures 3.4 and 3.5 were constructed from the logged data of the Steckel Mill under consideration.

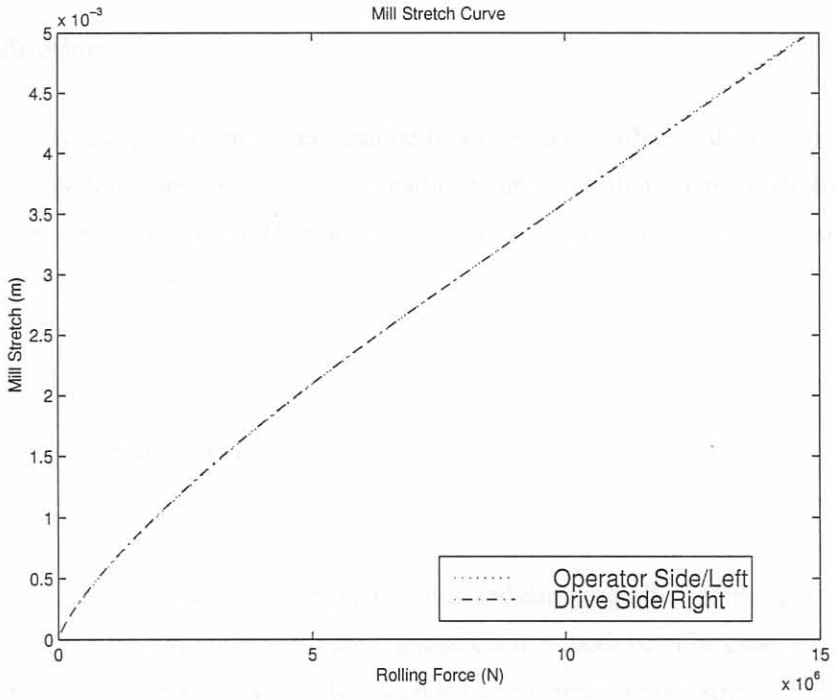

Figure 3.4: Mill stretch curves.

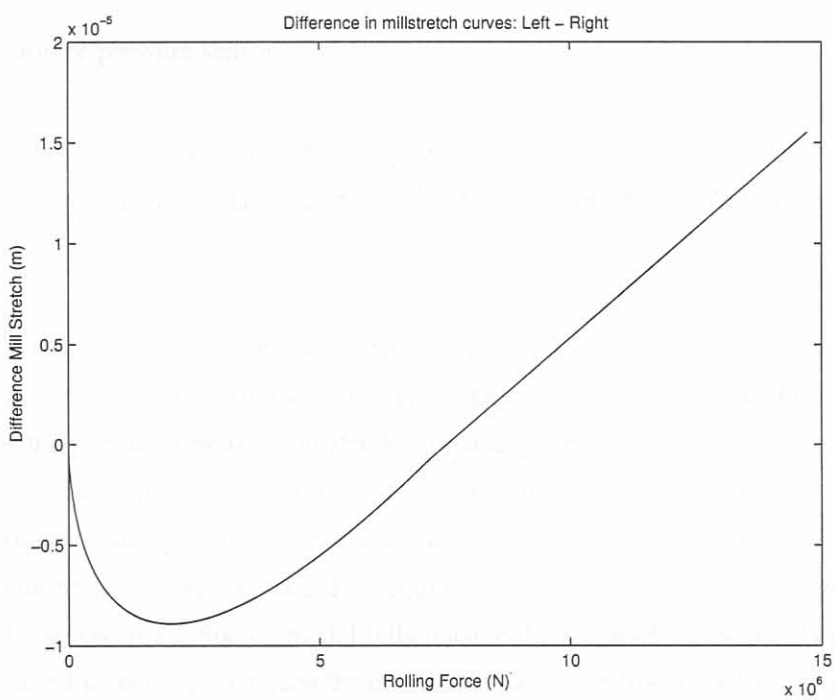

Figure 3.5: Difference in mill stretch curves.

3.6 The Hydraulic Actuator

3.6.1 Introduction

A hydraulic actuated gauge control system can be modelled with different degrees of detail [8]. The hydraulic actuator system consists of 6 major dynamic components that can be modelled to capture the nonlinear dynamic behaviour of the **H**ydraulic **A**ctuator **G**auge **C**ontrol (HAGC) system [8, 64, 65]. The components are as follows:

1. The servovalve.
2. The hydraulic transmission line.
3. The hydraulic cylinder.
4. The mill (dynamics, natural frequency, modulus and damping effect forming a compliant structure [66]). Guo [8] states that a complete gauge control model can be established if the rolling force terms, used in his study, can be extended to incorporate the strip deformation process, tension control loop and the drive control system. All the models that are mentioned by Guo, i.e. Roll Gap Model and the Tension Model, are modelled in this work, except for the drive control system.
5. The return line.
6. The position or pressure sensor.

The complexity of the model can be reduced by omitting some of the dynamic components, as was done by other researchers investigating the hydraulic AGC system [59, 64]. In this work the following components are omitted:

1. Transmission Line: The transmission line's dynamic effect can be omitted, because in modern designs the pressure line is kept as short as possible, typically shorter than 3 m (10 ft.). In some instances the pressure line is eliminated by mounting the servovalve directly onto the cylinder [8]. This assumption was also made by other researchers [59, 64]. Bhowal [64] stated that the transmission delay of the hydraulic oil in the pipe line is small and can be neglected. If an accurate transmission line model is required, the partial differential flow equations would have to be solved [67]. Such a model falls outside the scope of this work. Guo modelled the transmission line but approximated the distributed parameter line model as a lumped parameter line model [8]. The conclusion reached was that the transmission line provides extra damping in the hydraulic circuit, similar to a hydraulic accumulator.

2. Return Line: The return line was also neglected using the same train of thought followed for the transmission line modelling.

3. Sensor: The sensor can be modelled as a first order measuring system [8], but for this work the dynamics of the sensor were omitted and the sensor was modelled as a gain.

3.6.2 Modelling of the dynamic components

3.6.2.1 Operation

The servovalve assembly consists of a torque motor, hydraulic amplifier and a valve spool (figure 3.6). In [66] the working of the widely used two stage electro-hydraulic Moog Servovalve is described[11]. The input control current signal is converted to a mechanical signal, by causing a rotation of the armature to which a flapper arm is rigidly connected. The armature and flapper are supported by a thin-wall flexure sleeve. When the armature and flapper rotate about the flexure sleeve support, the spool is moved. The flapper closes off one nozzle and diverts the flow through that end of the spool. The spool moves and opens P_{high} to one control port and the other is opened to the other control port P_{low}. The spool pushes the ball end of the feedback spring creating a restoring torque on the armature-flapper connection. As the feedback torque becomes equal to the torque of the magnetic forces on the armature, the armature-flapper moves back to the centered position. The spool stops at a position where the feedback spring torque equals the torque due to the control input current. Therefore, the spool position is proportional to the input current.

The control ports are connected to either hydraulic transmission lines or directly to the hydraulic cylinder chamber entrances. By channeling flow in and out of the chambers the pressure in the chamber can be increased or decreased. The limits of the hydraulic circuit are P_{high} and P_{low}. Losses are encountered over transmission lines but in this dissertation such losses are not modelled. The interested reader is referred to [67, 66] which are references dealing with the field of hydraulic servosystems. Similar actuators were modelled for the left and the right side of the mill. The two actuators interact with the stand model as can be seen in figure 3.3.

3.6.2.2 Servovalve

The servovalve was modelled as a second order system and it is reported by Guo that this type of modelling agrees with test results obtained [8]. It is, however, reported elsewhere that it is difficult to model the servovalve with a simplified transfer function model due to the high-order non linear nature of its response [65]. The response of servovalves are functions of both the servovalve current and the pressure drop across the valve. It is suggested [65] that the frequency response curve of the

[11] A description of the working of such a servovalve can also be found on Moog's URL (http:/www.moog.com)

servovalve under investigation be obtained from its manufacturer, such as Moog and Bosch, when a suitable transfer function needs to be derived for the valve.

The chosen model can be written as,

$$\ddot{x}_{v_s} + 2\zeta_{v_s}\omega_{v_s}\dot{x}_{v_s} + \omega_{v_s}^2 x_{v_s} = \frac{\omega_{v_s}^2 x_{v_{smax}}}{I_{o_s}} I_{c_s}, \tag{3.77}$$

where the index $s \in [L, R]$ and,

x_{v_s}: Servovalve opening (spool movement);

$x_{v_{smax}}$: The maximum spool movement;

ω_{v_s}: Servovalve natural frequency (51Hz);

ζ_{v_s}: Servovalve damping ratio;

I_{c_s}: Controlled input current;

I_{o_s}: Rated servovalve current.

The controlled input current is calculated by assuming a cascaded proportional integral controller structure,

$$I_{c_s} = K_{c_s}\left((x_{sp_s} - x_s) + \frac{1}{\tau_{i_s}}\int_0^t ((x_{sp_s} - x_s)d\tau\right), \tag{3.78}$$

where K_{c_s} and τ_{i_s} is the gains of the controller and will be given chapter 4.

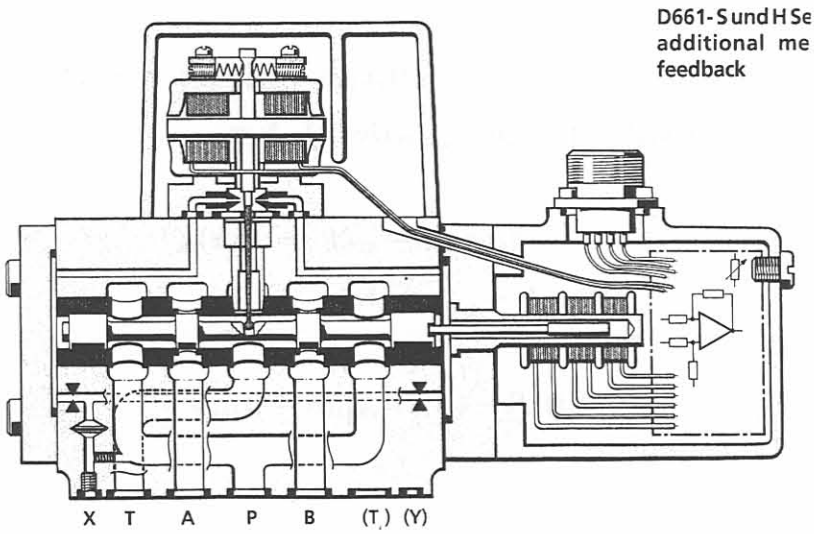

Figure 3.6: Hydraulic cylinder servovalve system (figure adapted from [68]). The top element is the torque motor, the horizontal bar channelling the flow is the servovalve spool and the vertical sleeve that moves the spool is the flexure sleeve.

3.6.2.3 Hydraulic cylinder

The hydraulic actuator being modelled is assumed to be double acting. This means that the stroke of the cylinder can be extended and contracted using the hydraulic fluid, while the mechanical stand system also influences the stroke. For a single acting hydraulic cylinder the stroke can only be extended and the stroke has to be decreased manually, for example by pushing the upper roll chocks upwards.

The cylinder pressure on either side of the cylinder are determined by four flow rates [8, 69]:

1. Cylinder flows ($Q_i \propto x_v\sqrt{\Delta P}, \forall i \in [1,2]$)
2. Leaking flow ($Q_l \propto (P_1 - P_2)$)
3. Volume change rate due to compressed oil ($Q_c = \frac{V}{\beta}\dot{P}$)
4. Flow rates due to the piston velocity ($Q_v = A\dot{x}$)

For the construction of the continuity equations the direction of positive cylinder flow is defined as flow into both chambers and the leakage flow from chamber 1 to chamber 2 (see Fig. 3.3). Constructing the continuity equations for the servo system yield [67, 69] the following:

$$Q_{s1}(t) = Q_{sl}(t) + \frac{V_{s1}(x_s)}{\beta_o}\dot{P}_{s1}(t) + A_{s1}\dot{x}_s(t); \tag{3.79}$$

$$-Q_{s2}(t) = -Q_{sl}(t) + \frac{V_{s2}(x_s)}{\beta_o}\dot{P}_{s2}(t) - A_{s2}\dot{x}_s(t); \tag{3.80}$$

$$\begin{aligned} V_{s1}(x_s) &= V_{01s} + A_{s1}x_s(t) \\ &= A_{s1}(stroke_{max_s} - h_{2_{setup}}) + A_{s1}x_s(t); \end{aligned} \tag{3.81}$$

$$\begin{aligned} V_{s2}(x_s) &= V_{02s} - A_{s2}x_s(t) \\ &= A_{s2}h_{2_{setup}} - A_{s2}x_s(t); \end{aligned} \tag{3.82}$$

$$Q_{ls}(t) = K_{leak_s}(P_{s1}(t) - P_{s2}(t)), \tag{3.83}$$

where,

Q_{s1}: Cylinder flow into the piston side chamber of the cylinder;

Q_{s2}: Cylinder flow into the rod side piston side chamber of the cylinder;

Q_{sl}: The leak flow from the piston side to the rod side of the cylinder;

P_{s1}: Cylinder pressure at the piston side of the cylinder;

P_{s2}: Cylinder pressure at the rod side of the cylinder;

x_s: The hydraulic stroke movement;

K_{leak_s}: Leakage flow coefficient;

β_o: Oil bulk modulus.

3.6.2.4 Operation and interaction with stand model

There are two cases to investigate, namely when the servovalve is charging ($x_{v_s} \geq 0$) and when the servovalve is dumping ($x_{v_s} < 0$). When $x_{v_s} \geq 0$ the cylinder flows are expressed as,

$$Q_{s1}(t) = K_{v_s} x_{v_s}(t) \sqrt{\frac{2}{\rho_o}(P_{high} - P_{s1}(t))}, \tag{3.84}$$

$$Q_{s2}(t) = K_{v_s} x_{v_s}(t) \sqrt{\frac{2}{\rho_o}(P_{s2}(t) - P_{low})}, \tag{3.85}$$

where,

P_{high}: The supply pressure of the hydraulic circuit at the high pressure side;

P_{low}: The tank pressure at the low pressure side of the hydraulic circuit;

ρ_o: Density of the hydraulic oil.

When $x_{v_s} < 0$, the leakage flow equation is kept unchanged and the flow leakage is predicted to be from the piston side to the rod side of the cylinder. The directions of the cylinder flows Q_{s1}, Q_{s2} are reversed. The cylinder flows when $x_{v_s} < 0$ are,

$$Q_{s1}(t) = K_{v_s} x_{v_s}(t) \sqrt{\frac{2}{\rho_o}(P_{s1}(t) - P_{low})}, \tag{3.86}$$

$$Q_{s2}(t) = K_{v_s} x_{v_s}(t) \sqrt{\frac{2}{\rho_o}(P_{high} - P_{s2}(t))}, \tag{3.87}$$

and x_s decreases.

The hydraulic actuator interacts with the stand model and the rolling mill frame. The thrust force of the hydraulic cylinder on either side of the mill is,

$$P_{s1}(t)A_{s1} - P_{s2}(t)A_{s2} = F_{HAs}(t). \tag{3.88}$$

Under steady state this force has to balance the transmitted rolling force on either side of the mill. The hydraulic actuator is top mounted for the configuration under investigation. This type of mounting results in a floating actuator base and the amount of floating is determined by the mill stretch.

The hydraulic stroke is increased to combat the amount of stretch and to maintain thickness control. The following relationship exists between the movement of the upper roll pack, hydraulic stroke and mill stretch,

$$x_s(t) = y_{stretch_s}(t) - y_1(z,t), \tag{3.89}$$

where $y_1(z,t) = y_{sT}(t)$ is such that, when $s = L \Rightarrow z = -\frac{l_1}{2}$ and $s = R \Rightarrow z = \frac{l_1}{2}$ (see figure 3.1). The stretch of the mill is a nonlinear function of the rolling force and strip width [59, 27, 3, 1] but with a predominant linear region. The stretch in the linear range of the mill stretch curve can be calculated as,

$$y_{stretch_s}(t) = \frac{(P_{s1}(t)A_{s1} - P_{s2}(t)A_{s2}) - F_{roll_{test_s}}}{K_{sT}} + y_{stretch_{test_s}}. \tag{3.90}$$

From figure 3.4 the mill stretch is seen to be predominantly a linear function of the applied force and Eq. 3.90 can be modified as follows,

$$y_{stretch_s}(t) \approx \frac{(P_{s1}(t)A_{s1} - P_{s2}(t)A_{s2})}{K_{sT}}. \tag{3.91}$$

Taking the derivative of the hydraulic stroke relationship (Eq. 3.89) and substituting the derivative of Eq. 3.90 into it, yields the velocity of the hydraulic stroke,

$$\dot{x}_s(t) = \frac{\dot{P}_{s1}(t)A_{s1} - \dot{P}_{s2}(t)A_{s2}}{K_{sT}} - \dot{y}_1(z,t). \tag{3.92}$$

The hydraulic cylinder rod velocity, $\dot{x}_s$, contains two pressure derivatives, Eq. 3.92. Substituting Eq. 3.92 into equations 3.79 and 3.80 yields,

$$Q_{s1}(t) = Q_{sl}(t) + \frac{V_{s1}(x_S)}{\beta_o}\dot{P}_{s1}(t) + A_{s1}\left(\frac{\dot{P}_{s1}(t)A_{s1} - \dot{P}_{s2}(t)A_{s2}}{K_{sT}} - \dot{y}_{s1}(z,t)\right), \tag{3.93}$$

$$-Q_{s2}(t) = -Q_{sl}(t) + \frac{V_{s2}}{\beta_o}\dot{P}_{s2} - A_{s2}\left(\frac{\dot{P}_{s1}(t)A_{s1} - \dot{P}_{s2}(t)A_{s2}}{K_{sT}} - \dot{y}_{s1}(z,t)\right). \tag{3.94}$$

Rearranging Eq. 3.94 making $\dot{P}_{s2}(t)$ the subject gives,

$$\dot{P}_{s2}(t) = \frac{-Q_{s2}(t) + Q_{sl}(t) - A_{s2}\dot{y}_{s1}(z,t) + \frac{\dot{P}_{s1}(t)A_{s1}A_{s2}}{K_{sT}}}{\left(\frac{V_{s2}(x_s)}{\beta_o} + \frac{A_{s2}^2}{K_{sT}}\right)}. \tag{3.95}$$

Defining, $\Delta = \frac{V_{s2}(x_s)}{\beta_o} + \frac{A_{s2}^2}{K_{sT}}$, and substituting Eq. 3.95 into Eq.3.93 yields,

$$\dot{P}_{s1}(t) = \frac{Q_{s1}(t) - Q_{sl}(t) + A_{s1}\dot{y}_{s1}(z,t) - \frac{A_{s1}A_{s2}}{K_{sT}\Delta}\left(Q_{s2} - Q_{sl} + A_{s2}\dot{y}_{s1}(z,t)\right)}{\frac{V_{s1}(x_s)}{\beta_o} + \frac{A_{s1}^2}{K_{sT}} - \frac{(A_{s1}A_{s2})^2}{K_{sT}^2\Delta}}. \tag{3.96}$$

The interactions between the linear stand model, the rolling mill frame and the hydraulic actuator have been adequately derived for the purpose of the mill simulator. These models will be expressed as a total nonlinear interacting state space model shown in chapter 4.

3.7 Temperature modelling

3.7.1 Introduction

In section 3.2 it is motivated why the heat transfer problem of the hot rolling process will not be solved. Measures taken in this dissertation to compensate for this lack of modelling are also discussed in section 3.2, and this entails using practical measured data of the Steckel mill process, and conditioning this data to form inputs to the mill simulator. In this section, however a brief introduction to temperature modelling of the hot rolling process will be given as an initiation of future modelling projects.

The Steckel mill is divided into five distinct temperature zones. These zones can be described as follows:

1. The pay-off coiler furnace
2. The radiation and convection zone of the strip before entrance into the roll gap
3. The roll gap
4. The radiation and convection zone of the strip after exit from the roll gap[12]
5. The take-up coiler furnace

The main aim of the temperature model is to calculate a more accurate temperature prediction of the temperature in the roll gap. The temperature in the roll gap influences the flow stress as well as the yield stress of the rolled material in the roll gap as can be seen in Eq. 3.25.

The modelling of the thermal behaviour of the rolling environment can be very involved as can be seen from numerous publications [30, 32, 33, 70]. The following assumptions can be made during the modelling stage in order to decrease the computation time needed to solve the implicit finite difference heat problem:

1. Disturbance variations of the input gauge does not influence the grid.
2. The deviations of the setup draft due to mill stretch etc. does not influence the grid
3. It is assumed that the temperature distribution over the width of the sheet remains constant. This can be motivated from the fact that the width of the sheet is much greater than the thickness and that the heat conduction in the transverse direction can be ignored [70].

[12]The modelling of these zones is straight forward and a static heat conduction PDE is solved with a transformation, $x = vt$ with x is the rolling direction, in order to find the dynamic model [30].

3.7.2 Roll gap temperature modelling

Yuen [32] studied the heat transfer problem found in the roll gap while rolling, by modelling a moving three layer composite strip, compressed between two rotating cylinders. The three layers that were investigated were the rotating rolls, the scale layer and the strip. For this model the scale layer was ignored, because the main aim was to keep the temperature model simple and only compute a more accurate temperature prediction in the roll gap as an input to the roll gap model.

Assuming the coordinate system is fixed in space and the material properties are constant in the temperature range under consideration, then the following heat transfer equation can be constructed for the two body system (strip and rollers).

$$\rho_i c_i \overline{v_i} \bullet \nabla T_i = k_i \nabla^2 T_i + Q_i \tag{3.97}$$

Where the index $i \subset [r, s]$, where r is used to indicate the rollers and s to indicate the strip.

When Eq.3.97 is developed, the following two heat conduction equations are found [32].

$$v_{sx}\frac{\partial T_s}{\partial x} + v_{sy}\frac{\partial T_s}{\partial y} = \alpha_s\left[\frac{\partial^2 T_s}{\partial x^2} + \frac{\partial^2 T_s}{\partial y^2}\right] + \frac{Q_s}{\rho_s c_s} \tag{3.98}$$

$$v_{rr}\frac{\partial T_r}{\partial r} + v_{r\theta}\frac{\partial T_r}{\partial \theta} = \alpha_r\left[\frac{\partial^2 T_r}{\partial r^2} + \frac{1}{r}\frac{\partial T_r}{\partial r} + \frac{1}{r^2}\frac{\partial^2 T_r}{\partial \theta^2}\right] + \frac{Q_r}{\rho_r c_r} \tag{3.99}$$

The boundary value problem, can be solved numerically with the aid of finite element methods or finite differences methods.

3.7.3 Coiler furnace models

The modelling of the coiler furnace is necessary if the temperature history of the sheet is of importance at any given time. The Steckel Mill employs multiple passes to achieve the desired reduction. Thus, the sheet is coiled on either side of the rolling mill twice or thrice before the strip's final thickness is reached. If the final aim of the research is the operation of a control system for all the passes, then these models might be necessary.

The strip is subjected to cooling during the pass and after it is wound on a coiler inside a furnace. Here the strip's temperature loss is to be minimized. A complicating factor is the conduction between adjacent sheet wraps that changes the boundary conditions of the heat transfer problem [38].

3.7.4 Thermal crown modelling

The thermal crown build-up on the rollers is not modelled in this dissertation. In [37] a basic two dimensional model is given that can be used to model the thermal crown build-up. The temperature of the rolls is between 15 - 60 °C and the average value of the crown is from 0.01-0.5 mm. The evolution of the thermal crown on the rollers is a slower process than the stand, actuator and tension model dynamics derived in this section. It is assumed that these slow dynamics will not be identifiable on the time scale under investigation.

3.8 Conclusion

In this section the mathematical theory of the nonlinear and linear models embodied in the mill simulator was derived. The models which the simulator consists of are the roll gap model, stand model, hydraulic actuator models and the tension models. The roll gap model is seen as the connecting model of the simulator. The identified inputs of the stand model are the thrust forces of the hydraulic actuators and the rollforce, which is an output of the roll gap model. The roll gap entry and exit speeds are also outputs of the roll gap model and these speeds serve as inputs to the tension models. In the following chapter the solution methodology associated with each of these models will be discussed, as well as the final model incorporation of the nonlinear plant simulator.